INTERNATIONAL JOURNAL FOR NUMERICAL METHODS IN FLUIDS
Int. J. Numer. Meth. Fluids 2002; **38**:1091–1110 (DOI: 10.1002/fld.262)

Transition and heat transfer predictions in a turbine cascade at various free-stream turbulence intensities through a one-equation turbulence model

G. I. Tsourakis, D. G. Koubogiannis and K. C. Giannakoglou*,†

Laboratory of Thermal Turbomachines, National Technical University of Athens, 9, Iroon Polytechniou Str., Zografou, Athens 15780, Greece

SUMMARY

The one-equation Spalart–Allmaras turbulence model, coupled with criteria for the prediction of the transition onset, is employed for the numerical prediction of the heat transfer along the nozzle guide vanes of a high-pressure turbine, at various operating conditions. Emphasis is put on how to overcome a known shortcoming of the Spalart–Allmaras model, i.e. its insensitivity to free-stream turbulence. For this purpose, an extra viscosity coefficient is defined and used in the mean flow equations. This extra viscosity is proportional to the free-stream turbulence with a damping in the boundary layer. Its use is adequate to circumvent the aforementioned weakness of the Spalart–Allmaras model, without any other intervention in the model itself. For the prediction of the onset of transition, the Abu-Ghannam and Shaw and the Mayle criteria are used, depending on the level of free-stream turbulence. Both yield very satisfactory predictions in a wide range of Reynolds numbers and/or turbulence intensities. From a numerical point of view, this paper proposes techniques for the implementation of the solution method on unstructured grids with triangular elements and reconfirms findings of previous works, like the suitability of the containment-circle tessellation in highly stretched grids. Copyright © 2002 John Wiley & Sons, Ltd.

KEY WORDS: transition; Spalart–Allmaras turbulence model; free-stream induced viscosity; unstructured grids; turbine flows; heat transfer

1. INTRODUCTION

Turbine flows are characterized by strong adverse and favorable pressure gradients as well as transition to turbulence and/or laminarization processes. The laminar boundary layer, which starts developing at the leading edge, is likely to undergo transition due to the effect of free-stream turbulence (the so-called 'by-pass' transition [1]). In turbomachinery flows, the high level of free-stream turbulence often by-passes the generation and amplification of two-

*Correspondence to: K. C. Giannakoglou, Laboratory of Thermal Turbomachines, National Technical University of Athens, 9 Iroon Polytechnion Str., 15780 Athens, Greece.
†E-mail: kgianna@central.ntua.gr

Received 27 March 2001
Revised 7 September 2001

dimensional instabilities (i.e. the mechanism which is responsible for the so-called 'natural' transition) and the turbulence spots are formed due to free-stream turbulence. This is reasonable since the flow entering the turbine comes from the combustor and is strongly turbulent. Incoming turbulence contributes to an earlier transition and the increase in heat transfer along both the laminar and the turbulent part of the flow. On the other hand, in transonic turbines, the formation of a shock wave, usually emanating from the trailing edge and reflecting on the suction side of the adjacent blade, is an alternative reason for the onset of transition.

A series of papers addressing the numerical prediction of turbine flows at high-subsonic and transonic flow conditions, through several turbulence and transition models, appeared in the literature. Some of them, especially those dealing with the same turbine to the one analyzed herein, will be cited as the paper develops.

The present work aims to analyze the predictive capabilities of the one-equation Spalart–Allmaras (SA) turbulence model for the analysis of a typical turbine cascade, at different Reynolds numbers and/or free-stream turbulence intensities. The case that will be analyzed is the VKI high-pressure turbine 2D nozzle guide vane [2]. This case is well documented and quite a few measurements over a wide range of flow conditions are available to support several parametric studies. The blade temperature remains constant and the comparison of predicted and measured heat transfer distributions along its contour is an excellent test for evaluating the capabilities of any numerical tool to predict transition and to capture the behavior of both laminar and turbulent boundary layers.

In the past, algebraic turbulence models (the Baldwin–Lomax [3–6] or the Mitchel one [7]), one-equation models (the Spalart–Allmaras one [5, 7]) and two-equation ($k-\varepsilon$ or $k-\omega$ ones, see References [6–8]) have been used for the analysis of the same problem. In some of these works, criteria for the prediction of the onset of transition based on integral boundary layer quantities (the Abu-Ghannam and Shaw [9] or the Mayle model [1], which are both used in this work) or the integration of the growth rates of instability waves (the so-called e^N model [4]) have been used. A few works in which the onset of transition was defined by the user can also be found (for instance Reference [5], using the SA model). As far as transition criteria are concerned, the previous works have shown that none of the aforementioned ones is clearly superior. When transition occurs over the rear part of the suction side its location is, in general, well predicted by the transition models. This is the case of incoming flow with low turbulence intensity. By increasing the free-stream turbulence intensity, turbulence models which cannot account for it (like the conventional SA model) or even models that are in principle sensitive to it (like $k-\varepsilon$ or $k-\omega$ models) tend to underpredict the heat transfer distribution along the laminar part of the boundary layer and this also affects the location of the transition point.

In this paper, the SA model is employed coupled with the Abu-Ghannam and Shaw (for low free-stream turbulence intensity) and the Mayle (for high free-stream turbulence intensity) transition criteria. An enriched 'variant' of the conventional SA model is devised, where the free-stream turbulence effect is taken into account using an extra viscosity coefficient. By doing so, excellent predictions of the heat transfer distributions along both the pressure and suction sides of the turbine blade are obtained, in a wide range of Reynolds numbers and free-stream turbulence intensities. The turbine cascade is discretized using an unstructured grid with triangular elements. This causes practical difficulties related to the implementation of the transition criteria which are discussed along with the proposed remedies.

2. GOVERNING EQUATIONS

The Favre-averaged Navier–Stokes equations

$$\frac{\partial \mathbf{W}}{\partial t} + \frac{\partial \mathbf{F}_i^{inv}}{\partial x_i} - \frac{\partial \mathbf{F}_i^{vis}}{\partial x_i} = \mathbf{0} \tag{1}$$

are solved along with the state equation for perfect gases and the SA turbulence model [10]. In Equation (1), $\mathbf{W}=(\rho, \rho u_1, \rho u_2, E)^T$ stands for the solution variables array, any repeated index implies summation and $\mathbf{F}_i^{inv}$, $\mathbf{F}_i^{vis}$, $i=1,2$ stand for the inviscid and viscous fluxes, respectively. The cartesian velocity components are denoted by u_i, $i=1,2$.

The SA model consists of a single partial differential equation for the quantity $\tilde{\mu}$, from which the turbulent viscosity coefficient is derived as follows

$$\mu_t = f_{v1}\tilde{\mu}, \quad f_{v_1} = \frac{\chi^3}{\chi^3 + c_{v_1}^3}, \quad \chi = \frac{\tilde{\mu}}{\mu} \tag{2}$$

where μ is the bulk viscosity and $c_{v_1}=7.1$. Dealing with compressible flows, the equation originally proposed in Reference [10] for incompressible fluids, takes the form

$$\frac{\partial}{\partial t}(\rho\tilde{\mu}) + \frac{\partial}{\partial x_j}(\rho u_j \tilde{\mu}) = \frac{1}{\sigma}\left[\frac{\partial}{\partial x_j}\left((\mu+\tilde{\mu})\frac{\partial \tilde{\mu}}{\partial x_j}\right) + c_{b_2}\frac{\partial \tilde{\mu}}{\partial x_j}\frac{\partial \tilde{\mu}}{\partial x_j}\right] + S \tag{3}$$

The source term S is given by

$$S = c_{b_1}(1-f_{t_2})\tilde{S}\rho\tilde{\mu} - \left(c_{w_1} f_w - \frac{c_{b_1}}{\kappa^2} f_{t_2}\right)\left(\frac{\tilde{\mu}}{y}\right)^2 + \rho^2 f_{t_1}\Delta U^2 \tag{4}$$

where

$$\tilde{S} = \Omega f_{v_3} + \left(\frac{\tilde{\mu}}{\rho\kappa^2 y^2}\right) f_{v_2}, \quad f_{v_2} = \left(1 + \frac{\chi}{c_{v_2}}\right)^{-3}, \quad f_{v_3} = \frac{1}{\chi}(1+\chi f_{v_1})(1-f_{v_2}) \tag{5}$$

$$f_w = g\left(\frac{1+c_{w_3}^6}{g^6 + c_{w_3}^6}\right)^{1/6}, \quad g = r + c_{w_2}(r^6 - r), \quad r = \frac{\tilde{\mu}}{\tilde{S}\rho\kappa^2 y^2} \tag{6}$$

$$f_{t_1} = c_{t_1} g_t \exp\left[-c_{t_2}\frac{\Omega_t^2}{\Delta U^2}(y^2 + g_t^2 y_t^2)\right],$$

$$f_{t_2} = c_{t_3}\exp(-c_{t_4}\chi^2),$$

$$g_t = \min\left(0.1, \frac{\Delta U}{\Omega_t \Delta x}\right) \tag{7}$$

and $c_{v_2}=5$, $c_{b_1}=0.1355$, $c_{b_2}=0.622$, $\sigma=2/3$, $c_{w_2}=0.3$, $c_{w_3}=2$, $c_{w_1}=3.239$, $c_{t_1}=1$, $c_{t_2}=2$, $c_{t_3}=1.2$, $c_{t_4}=0.5$.

In the above equations, y stands for the distance from the nearest wall, Ω is the vorticity magnitude and $\kappa=0.41$ is the von-Karman constant. The updated values for some of the model constants proposed in Reference [11] and the expression for $\tilde{S}$ (Equation (5)) proposed in

Reference [12] have been adopted. The f_{t_1} and f_{t_2} functions (the subscript t stands for 'trip') simulate transition to turbulence, on condition however that a separate criterion (or the user themself) locates the trip point. Given the onset of transition, one may compute Ω_t (the vorticity magnitude at the trip point), ΔU (the difference between the velocity at any field point and that at the trip point) and Δx (the grid spacing along the wall at the trip). At the inlet, $\tilde{\mu}=0.001\mu$ regardless of the incoming turbulence intensity; along the solid walls $\tilde{\mu}=0$.

2.1. Modifications to account for free-stream turbulence

Originally, the SA model was proposed and tested [10] for external aerodynamics without being able to account for the effect of free-stream turbulence intensity τ_u. In turbomachinery applications, this effect should be taken into account and, for this reason, we propose the use of a third viscosity coefficient μ_{τ_u}, which is added to the effective viscosity ($\hat{\mu}_{\text{eff}}=\mu+\mu_t+\mu_{\tau_u}$) and used in the diffusion terms of the mean flow equations. In this way, an enriched SA model variant is devised without modifying the model equations. According to Reference [13], the free-stream induced coefficient μ_{τ_u} can be modeled algebraically. The expression for μ_{τ_u} was derived from References [13] and [14] after some modifications and reads

$$\mu_{\tau_u}=\alpha\rho_e u_e \tau_u \delta \left[\min\left\{1,\left(\frac{y}{\delta}\right)\right\}\right]^{\beta} \tag{8}$$

with $\alpha=0.2\sqrt{3}$ and $\beta=2.5$. The subscript 'e' denotes 'external' flow quantities, i.e. those computed at the edge of the boundary layer and δ stands for the boundary layer thickness. Practicalities about the computation of external quantities will be given in a subsequent section. In what follows, the proposed variant of the SA model, which employes Equation (8), will be denoted by SA(τ_u).

Equation (8) should be considered as the synthesis of the Volino [13] and the Forrest [14] approaches, though in the latter μ_{τ_u} is a linear function of the distance from the wall and its expression involves a coefficient which depends on the Pohlhausen's pressure gradient parameter (see Equation (15)) instead of the constant coefficient of Equation (8). Further modifications, like the one proposed by Boyle [15], according to which μ_{τ_u} is applied only when the flow is laminar, have not been adopted in the present work.

3. NUMERICAL SOLUTION METHOD

The governing equations are discretized on an unstructured grid with triangular elements using a node-centered, finite-volume technique and then solved through a time-marching scheme. Due to the fact that the grid is very stretched close to the solid walls where the triangles are extremely thin, this paper employs and compares two alternative control-volume definitions. Thus, the control-volume C_P around a grid vertex P is defined by successively connecting the midpoints of the edges incident upon P with (a) the barycenters (this will be referred to as fv-1, Figure 1), or (b) the centres of the containment circles (referred to as fv-2, Figure 2) of the surrounding triangles [16]. The two finite-volume formulations are shown in Figures 1 and 2. The second formulation presents certain advantages in very stretched grids, since the alignment of PQ and the normal vector $\mathbf{n_{PQ}}$ contributes to the minimization of false diffusion.

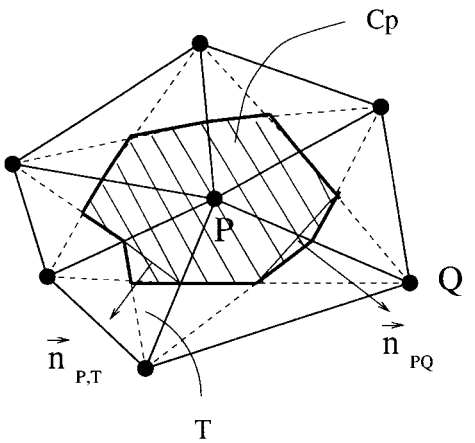

Figure 1. Median dual-tessellation (fv-1).

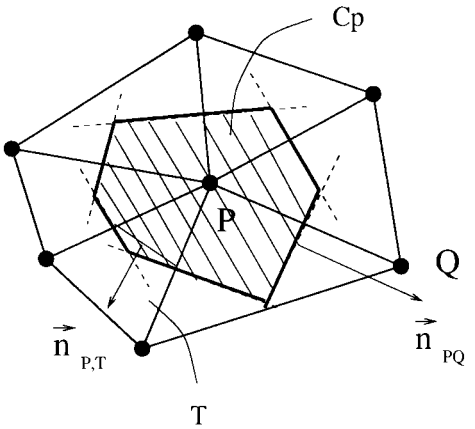

Figure 2. Containment dual-tessellation (fv-2).

The mean flow and turbulence equations are integrated over C_P and yield

$$\frac{\partial}{\partial t}\int\int_{C_P}\mathbf{W}\mathrm{d}x_1\mathrm{d}x_2+\oint_{\partial C_P}\mathbf{F}_n\,\mathrm{d}s=\int\int_{C_P}\mathbf{S}\,\mathrm{d}x_1\mathrm{d}x_2 \tag{9}$$

where ∂C_P is the boundary of C_P, and $\mathbf{F}_n=n_i\mathbf{F}_i/|\mathbf{n}|$.

In symbolic discrete form, the line-integral term in Equation (9) can be written as

$$\sum_{Q\in K_N(P)}\mathbf{\Phi}^{inv}(\mathbf{U}^L_{PQ},\mathbf{U}^R_{PQ},\mathbf{n}_{PQ})+\sum_{Q\in K_{\mathscr{T}}(P)}\mathbf{\Phi}^{vis}(\mathbf{U}_G,(\nabla\mathbf{U})_{\mathscr{T}},\mathbf{n}_{P,\mathscr{T}}) \tag{10}$$

where $\mathbf{U}=(\rho,u_1,u_2,p)^T$ is the primitive variables array, $K_N(P)$ and $K_T(P)$ are the sets of nodes and triangles around node P, respectively (see also Figures 1 and 2) whereas subscripts G and $\mathscr{T}$ denote barycenters and triangles. Equation (10) implies a different decomposition

of ∂C_P for the inviscid fluxes (on a per grid edge basis) and for the viscous ones (on a per triangle basis).

For the numerical calculation of $\mathbf{\Phi}^{vis}$, the primitive variables are assumed to vary linearly within each triangle, where $(\nabla U)_{\mathscr{T}}$ is thus constant. The inviscid fluxes are computed by means of the Roe flux-difference splitting scheme [17] as it applies between a left (L) and a right (R) state, defined on either side of a ∂C_P part (Figures 1 and 2). $\mathbf{\Phi}^{inv}$, $i=1,2$ are calculated with second-order accuracy through an extrapolation scheme applied to the primitive variables as follows [18]

$$\mathbf{U}^L=\mathbf{U}_P+\tfrac{1}{2}\mathbf{PQ}\cdot(\nabla\mathbf{U})_P,\quad \mathbf{U}^R=\mathbf{U}_Q-\tfrac{1}{2}\mathbf{PQ}\cdot(\nabla\mathbf{U})_Q \tag{11}$$

Equation (11) calls for the gradients of primitive variables over grid nodes. A standard way to obtain $(\nabla U)_P$ or $(\nabla U)_Q$ is through the Green–Gauss reconstruction. However, according to References [16] and [18], whenever stretched grids are used, the gradients used in Equation (11) should be computed using the least squares approximation. In stretched grids, the least squares-based computation greatly contributes in preserving the desired accuracy.

Local time stepping is used. The left-hand-side is derived using a first-order linearization of the right-hand-side. The solution variables are updated in a loosely coupled manner; first the mean flow (4×4 block system) and then the SA equation, both by means of the pointwise-implicit Gauss–Seidel scheme.

4. TRANSITION MODELLING

4.1. Criteria for the onset of transition

As already mentioned, the built-in trip terms f_{t1}, f_{t2} of the SA model simulate transition on condition that an 'external' criterion determines the transition onset. For this purpose, two different criteria are used in the present work, namely the experimental correlations of Abu-Ghannam and Shaw (AGS [9]) and that of Mayle [1]. Both have been used in the past for turbomachinery calculations, including the VKI turbine analyzed herein, though coupled with different turbulence models [4, 19]. Note that the transition end is not needed, since the transitional region is modeled through the SA trip terms. According to both correlations, transition occurs when the local Reynolds number $Re_\theta=\rho_e u_e\theta/\mu$, based on the momentum thickness θ, exceeds a critical value $Re_{\theta,\mathrm{crit}}$, namely

$$Re_\theta \geqslant Re_{\theta,\mathrm{crit}} \tag{12}$$

In the AGS correlation, $Re_{\theta,\mathrm{crit}}$ is given by

$$Re_{\theta,\mathrm{crit}}=163+\exp\left[F(\lambda_\theta)-\frac{F(\lambda_\theta)}{6.91}\,\tau_u\right] \tag{13}$$

where

$$F(\lambda_\theta)=\begin{cases}6.91+12.75\lambda_\theta+63.34\lambda_\theta^2 & (\lambda_\theta<0)\\ 6.91+2.48\lambda_\theta-12.27\lambda_\theta^2 & (\lambda_\theta\geqslant0)\end{cases} \tag{14}$$

The AGS model involves τ_u and the Pohlhausen's pressure-gradient parameter λ_θ

$$\lambda_\theta = \frac{\rho_e \theta^2}{\mu} \frac{\mathrm{d}u_e}{\mathrm{d}s} \tag{15}$$

where s stands for arclength. Originally, the AGS model was proposed for use in the range

$$-0.1 \leqslant \lambda_\theta \leqslant 0.1 \tag{16}$$

so that the computed λ_θ values are to be limited in this range [19].

On the other hand, Mayle proposed an alternative correlation to compute $Re_{\theta,\mathrm{crit}}$. According to Reference [1], $Re_{\theta,\mathrm{crit}}$ is expressed only in terms of the turbulence intensity, as

$$Re_{\theta,\mathrm{crit}} = 400 \cdot \tau_u^{-5/8} \tag{17}$$

for $\tau_u \geqslant 3$. The Mayle model should be used for high-τ_u while the AGS model for low τ_u. However, their application ranges overlap somewhat, so that at medium τ_u both values can be used. The two transition criteria are employed only if the acceleration parameter K, defined at each point along the blade surface as

$$K = \frac{\mu}{\rho_e u_e^2} \cdot \frac{\mathrm{d}u_e}{\mathrm{d}s} \tag{18}$$

is lower than 3×10^{-6} [1].

It should be mentioned that in separated boundary layers, the external velocity and the momentum thickness take locally almost constant values. Therefore the growth of Re_θ approaches zero and either the AGS or the Mayle model are likely to fail.

In Figure 3, numerically predicted distributions of the skin friction coefficient on a flat plate, obtained using SA and the aforementioned transition criteria, are shown. They correspond to $Re = 10^7$, $M_\infty = 0.2$ and $\tau_{u,in} = 1.5\%$ and are also compared to the Blasius (laminar) and power-law [20] curves.

4.2. Practical implementation of transition criteria

In transition criteria, the role of turbulence intensity (τ_u) is dominant. It is recommended [21] that local τ_u values should be used rather than free-stream ones, as follows

$$\tau_{u,l} = \frac{1}{u_e}(\tau_{u,in} \cdot u_{in}) \tag{19}$$

Another suggestion is that of Dunham [22], according to which the average of the local and the inlet values should be used

$$\tau_{u,av} = \tfrac{1}{2}(\tau_{u,in} + \tau_{u,l}) \tag{20}$$

Both approaches are discussed and assessed in the results section.

At each iteration, the transition model (AGS or Mayle) is employed prior to the numerical integration of the SA model. Through the criterion 12, the onset of transition for each side of the airfoil is located and its coordinates are communicated to the SA model; neither the transition length nor the intermittency factor (or any other quantity which could be computed by the AGS or the Mayle models) are needed. With the actual transition location, field values

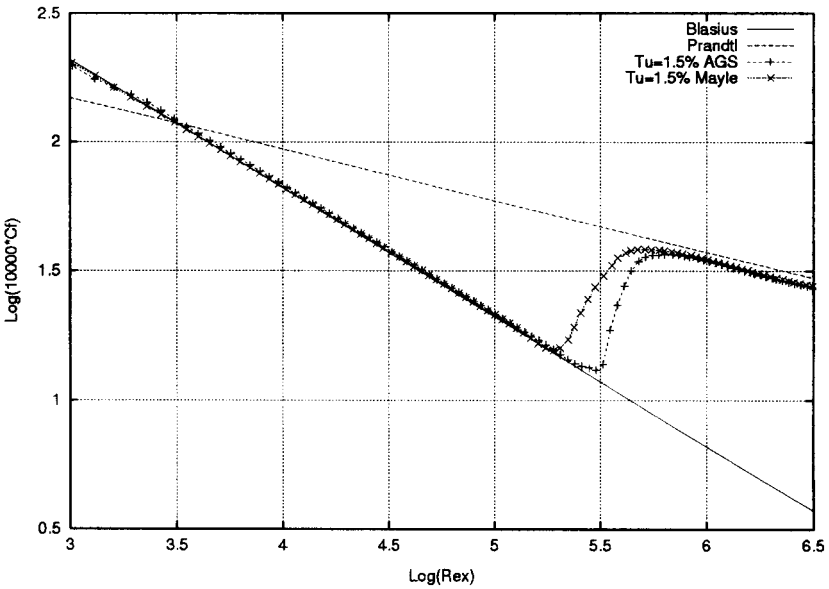

Figure 3. Friction coefficient along a flat plate for $M_\infty = 0.2$, $Re = 10^7$ and $\tau_{u,in} = 1.5\%$.

for f_{t_1} and f_{t_2} are computed (Equation (7)) and the numerical solution of Equation (3) provides the updated $\tilde{\mu}$ (and consequently μ_t) values over the computational nodes.

The transition criteria require an estimate of the boundary layer thickness δ for a number of reasons like, for instance, the computation of the momentum thickness θ and of the external velocity u_e. The complex velocity profiles arising in turbine flows prevent the use of the standard 99% definition. In the present study, the method of Rodi and Michellassi [19] was used, according to which the boundary layer edge at each cross section normal to the surface, is defined as the point where vorticity Ω equals

$$\Omega = \Omega_{\min} + 0.01 \cdot (\Omega_{\max} - \Omega_{\min}) \tag{21}$$

where $\Omega_{\min}$ and $\Omega_{\max}$ are its minimum and maximum values along the cross section.

From a practical point of view, such a computation is troublesome on unstructured grids. Simplifying assumptions, like that the transversal to the boundary grid lines can be considered to be vertical to them (frequently used with structured grids) are not generally applicable, even if a part of the grid in the vicinity of solid walls has been generated in a layered manner (Figure 7 later). Thus, vertical lines should be drawn at each nodal point on the walls (Figure 4). Flow quantities (velocity, density, vorticity) at the intersection of each vertical line with grid edges need to be computed and this is accomplished using Taylor expansions. The length of transversal lines that are to be drawn is a reasonable percentage of the cascade pitch (usually about 15–20%).

The above technique, coupled with the Michellassi method for the calculation of δ, resulted in a satisfactory estimate of the external velocity distribution $u_e(s)$, that is practically considered to be the parallel to the solid wall velocity at distance δ. Additionally, a smoothing

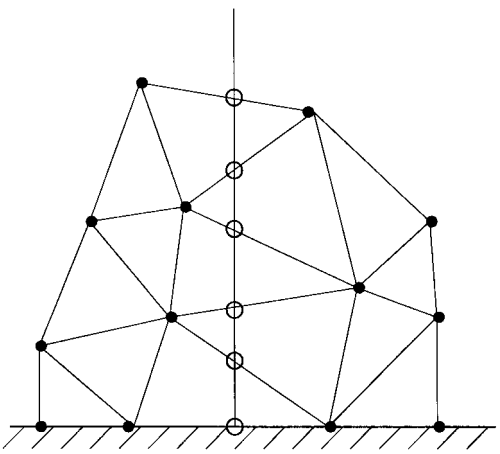

Figure 4. Transversal to the solid wall lines for the evaluation of velocity profiles.

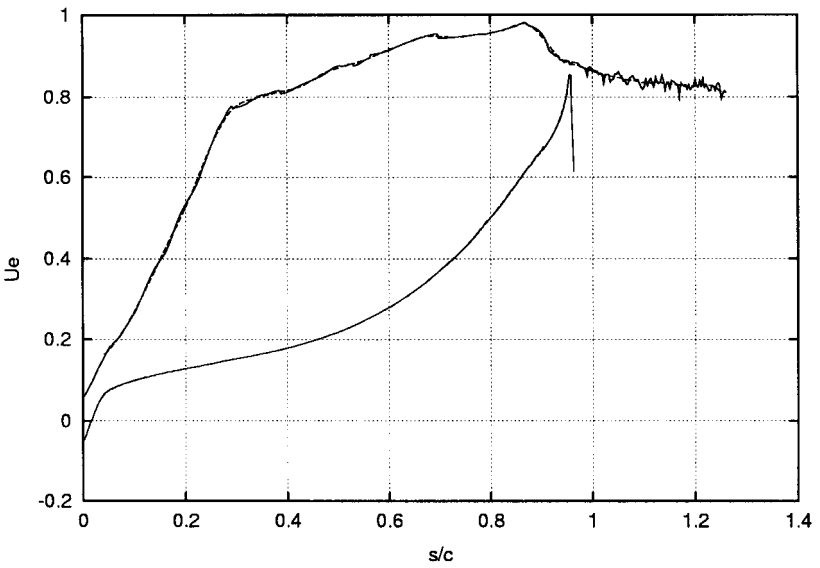

Figure 5. External velocity distribution along the blade (MUR235), before (continuous line) and after smoothing (dashed line).

procedure was found to be necessary in order to compute accurately the $\mathrm{d}u_e/\mathrm{d}s$ derivative (Figure 5), to be used in Equations (15) and (18).

Concerning the calculation of θ, this could be based upon its definition

$$\theta = \int_0^\infty \frac{\rho}{\rho_e}\frac{u}{u_e}\left(1-\frac{u}{u_e}\right)\mathrm{d}y \tag{22}$$

Alternatively, the method proposed by Reference [20] is used, originally proposed for incompressible fluids, which yields

$$\theta^2 \approx \frac{0.45\mu}{\rho_e u_e^6} \int_0^s u_e^5 \, \mathrm{d}s \tag{23}$$

5. RESULTS AND DISCUSSION

The numerical method described in this paper will be used to predict the heat transfer around the blades of a transonic linear turbine guide vane cascade, at various flow conditions. Aerodynamic and heat transfer measurements have been carried out in VKI and reported by Arts *et al.* [2]. During the experiments, several operating points were analyzed, all of them at zero inlet angle. The chord length is 67.65 mm, the solidity is 1/0.85 and the stagger angle 55 deg. The operating points, listed in Table I, are analyzed in the present study.

In each of these cases, the heat flux distribution $q_w(s)$ predicted along the blade contour is compared with the corresponding measurements. These distributions are expressed in terms of the heat transfer coefficient h, defined as

$$h = \frac{q_w}{T_{\text{tot}} - T_{\text{wall}}} \tag{24}$$

where T_{tot} and T_{wall} are the inlet total and the wall static temperatures, respectively.

The unstructured computational grid used is shown in Figure 6. It consists of 20 332 nodes, 39 868 triangles and numerical tests showed that it yields grid-independent results. In order to facilitate the implementation of the turbulence model in the vicinity of walls, a number of pseudo-structured grid layers were first generated around the airfoil. The remainder of the computational domain was filled with a purely unstructured grid. A close-up view of the final mesh, near the airfoil trailing edge, is presented in Figure 7. The grid stretching is such that

Table I. Summary of test cases, grouped in terms of inlet Reynolds number.

MUR	$M_{2,is}$	Re_{in} ($\times 10^5$)	τ_u (%)	T_{wall} (K)
239	0.922	4.92	6	299.75
245	0.924	4.91	4	300.75
247	0.922	4.87	1	302.15
235	0.927	2.65	6	301.15
232	1.061	2.42	6	302.15
213	1.068	2.41	4	298.25
210	1.076	2.43	1	297.35
129	0.840	2.71	0.8	297.75
222	1.134	1.20	6	301.95
224	0.927	1.36	6	302.05
226	0.920	1.34	4	301.65
228	0.933	1.36	1	302.85

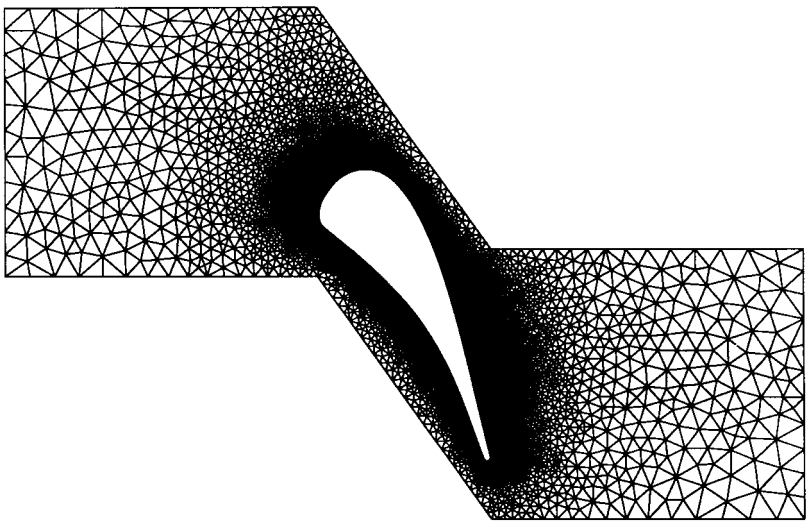

Figure 6. Computational grid.

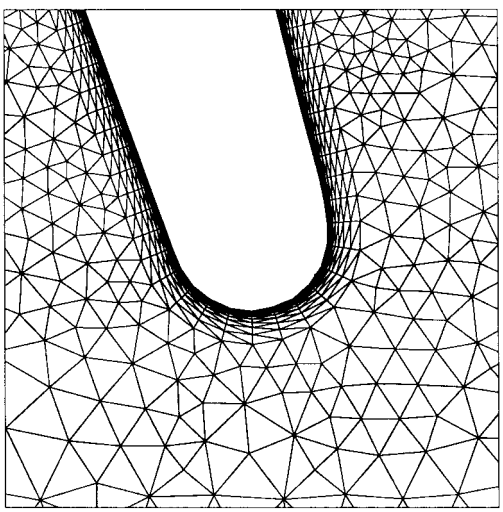

Figure 7. Pseudo-structured grid layers in the vicinity of solid walls.

the y^+ values of the first mesh points off the wall are below 1. Using the aforementioned grid, the mean flow and turbulence equations were able to converge to machine accuracy; a typical convergence history is shown in Figure 8.

The MUR235 case will be analyzed first by laying emphasis on the prediction of transition, using the AGS and Mayle models. The same case will be used to assess alternative ways for the computation of some of the involved quantities, as discussed in the previous sections. Conclusions from this will be applied in computations at other operating points as well. The

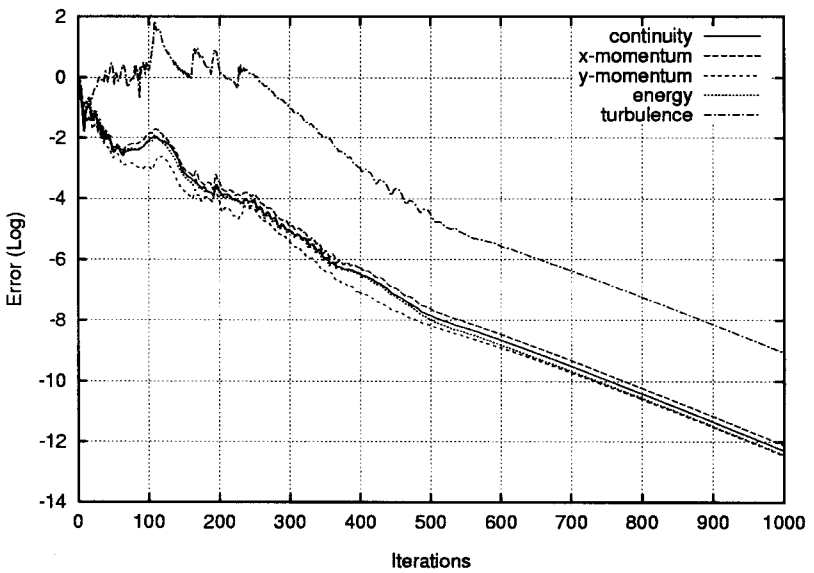

Figure 8. Typical convergence of the equations (MUR235).

external velocity distribution $u_e(s)$ is required by both transition criteria, since the computation of both θ and K depend upon this distribution. Inaccuracies linked to the computation of δ through the Michellassi technique and/or interpolations required to compute u_e are likely to yield non-smooth u_e distributions, like the one shown in Figure 5. The computation of K, according to Equation (18), is very sensitive to the smoothness of u_e as it involves its first derivative. The same sensitivity is associated with the λ_θ computation, Equation (15). In view of the above, the u_e distribution needs to be smoothed prior to its differentiation. The smoothed u_e distribution is also plotted in Figure 5, where a rapid flow acceleration along the first 25% of the suction side is observed. Further downstream, the acceleration becomes milder and is followed by an abrupt deceleration next to the trailing edge. The flow is accelerated on the pressure side, giving rise to a velocity distribution which is typical for this kind of turbine blade.

The distribution of K along the blade airfoil, computed through the smoothed external velocities, is illustrated in Figure 9. In the same figure, the value $K=3\times10^{-6}$, i.e. the threshold below which transition may occur, has been marked. It may be seen that, with the exception of the leading edge area, the major part of the suction side satisfies this criterion. According to both transition models, the momentum thickness is the parameter that mainly affects the onset of transition. For the MUR235 case, Figure 10 presents two differently computed distributions of θ over the airfoil contour, as shown in the previous section. On the pressure side, corresponding to negative arclength values, the momentum thickness increases along the leading part of the blade. Then, the strong favorable pressure gradient causes the flow to accelerate, thereby reducing the boundary layer thickness. On the suction side, θ increases continuously with a rate that becomes steeper after transition. A computation based on Equation (22) yields overestimated predictions compared to the ones obtained by Equation (23). The overestimation of θ affects the location of the onset of transition and, as a conse-

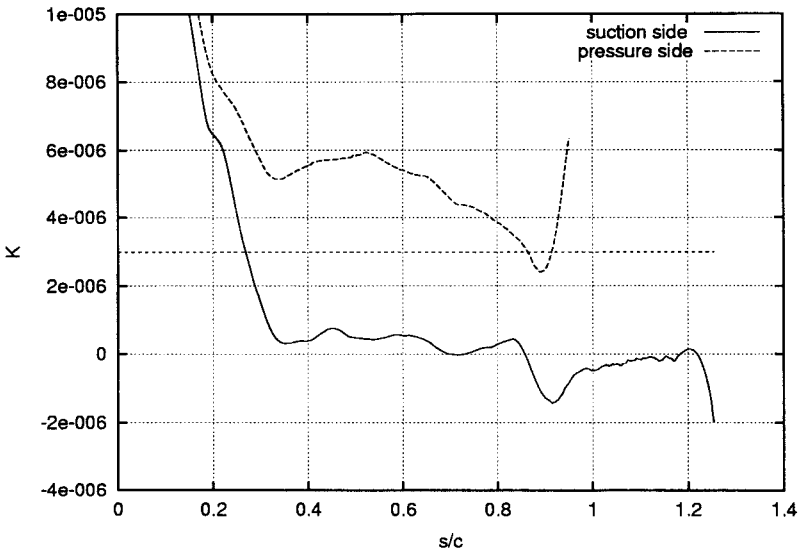

Figure 9. Distribution of the acceleration parameter K (MUR235).

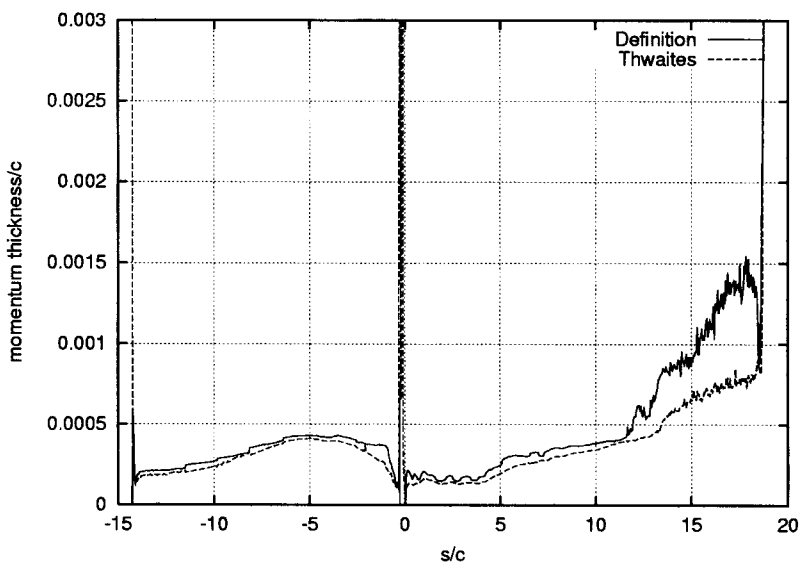

Figure 10. Distribution of momentum thickness (MUR235).

quence of Equation (12), this is differently predicted by the two models. Figure 11 presents the heat flux coefficient distribution along the airfoil and should be examined in relation to Figure 10. The Mayle model was used since the free-stream turbulence intensity is high. Three different implementations of this model are compared with measurements. Using the local τ_u to compute $Re_{\theta,\mathrm{crit}}$, the location of the transition is accurately captured. In contrast, the use of

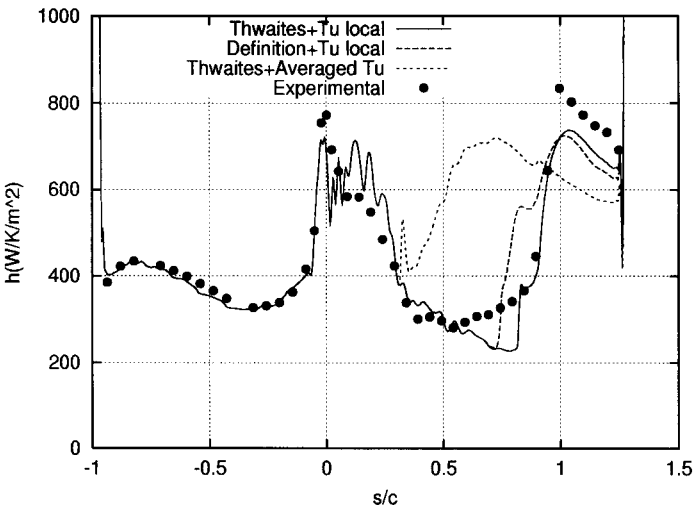

Figure 11. MUR235 ($Re = 2.65 \times 10^5, M_{2,is} = 0.927, Tu = 6.0$ per cent). Heat flux coefficient distributions (MUR235).

averaged $\tau_{u,av}$ values, Equation (20), predicts an unphysically early transition to turbulence. Thus, we reconfirm a previous statement by Hu and Fransson [21], about the appropriateness of using local τ_u values and in what follows, either with the AGS or the Mayle criterion, $Re_{\theta,\text{crit}}$ will be computed using local turbulence intensities.

The previous comparisons were all based on predictions obtained using the so-called SA(τ_u) model, as proposed in this paper. At this point, the role of adding the μ_{τ_u} coefficient in the diffusion terms in the mean flow will be investigated. The MUR235, MUR222 and MUR129 cases have been selected for this investigation and results are presented in Figures 12, 13 and 14, respectively. In the MUR235, the conventional SA model underpredicts the heat transfer coefficient on the laminar part of the flow (i.e. over the major part along the suction side and the entire pressure side), thus revealing its weakness in all high-τ_u cases (here, $\tau_u = 6\%$). With the SA(τ_u) model, the increase in h at the onset of transition is less abrupt compared to the very abrupt change obtained using the original SA model. From Figure 12, it is obvious that the use of an extra τ_u-sensitive viscosity coefficient is mandatory. In the MUR222 case, the τ_u is still high ($\tau_u = 6\%$) with a lower Reynolds number and higher exit Mach ($M_{2,is} = 1.134$). The improvement offered by the SA(τ_u) model over both airfoil surfaces is noticeable. The abrupt increase in the heat transfer rate on the suction side moves towards the trailing edge and its predicted location coincides with both the SA and the SA(τ_u). It is a pure trailing edge effect, so the two models behave identically in this area. In the MUR129 case, as in every other low-τ_u flow case, differences between SA and SA(τ_u) become almost negligible. A general conclusion is that the SA(τ_u) model generally improves the predictions over the entire contour of the airfoil and matches the available measurements.

The results shown in Figure 11 (MUR235) were all obtained using the containment-dual tesselation, i.e. the so-called fv-2 scheme. Figure 15 justifies this choice as it compares predictions through the two finite-volume definitions. The transition criterion which performed better according to Figure 11, was used. Figure 15 demonstrates the superiority of the fv-2 scheme,

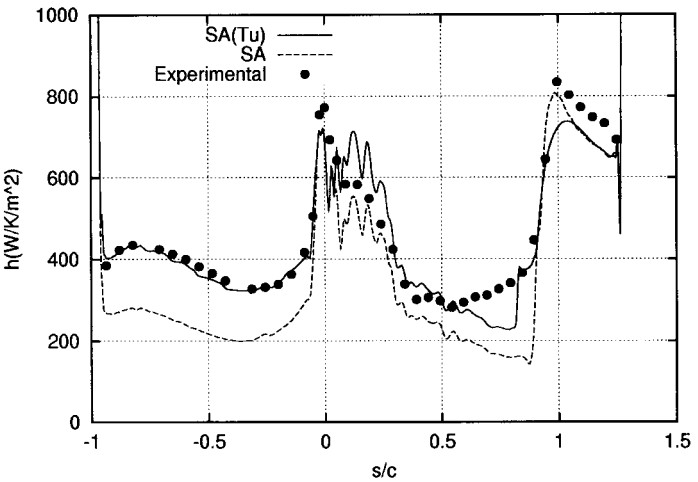

Figure 12. MUR235 ($Re = 2.65 \times 10^5$, $M_{2,is} = 0.927$, $Tu = 6.0\%$). Comparison of the conventional SA and the proposed SA(τ_u) model.

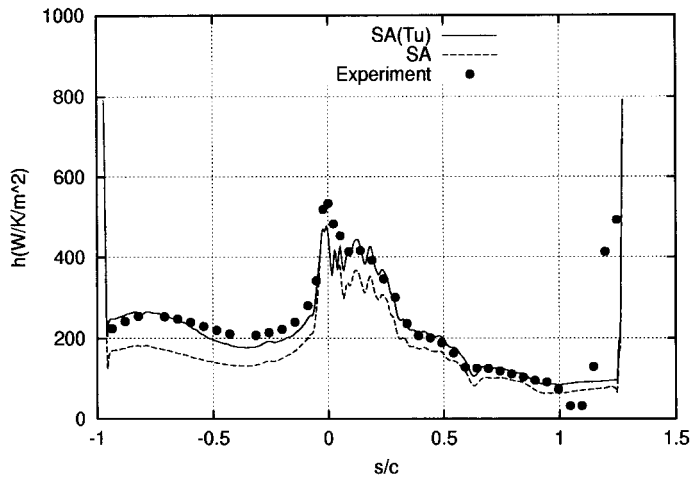

Figure 13. MUR222 ($Re = 1.20 \times 10^5$, $M_{2,is} = 1.134$, $Tu = 6.0\%$). Comparison of the conventional SA and the proposed SA(τ_u) model.

especially in the fully turbulent region. These conclusions were reconfirmed by repeating the same computations in the MUR247 case, Figure 16. Since MUR247 is characterized by low-τ_u, the AGS transition model was used. In this case, too, the containment-dual tesselation predicts the heat transfer along the blade very satisfactorily, whereas the median-dual tesselation yields discrepancies in the fully turbulent area, i.e. the last part of the suction side. Summarizing, Figures 15 and 16 indicate the pronounced effect of the finite-volume discretization scheme on the numerical solution of the governing equations.

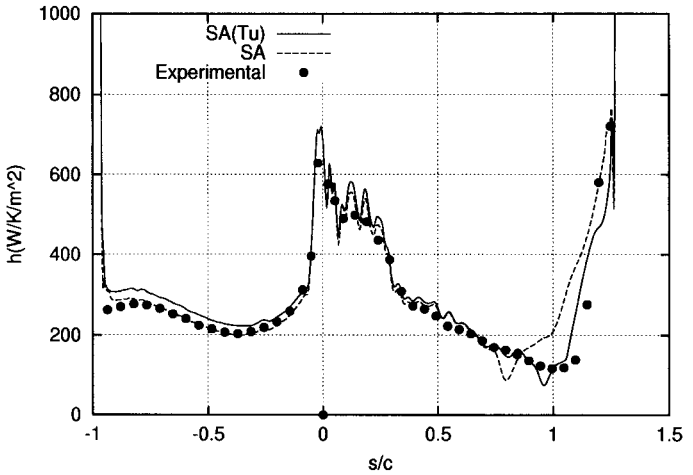

Figure 14. MUR129 ($Re = 2.71 \times 10^5$, $M_{2,is} = 0.840$, $Tu = 0.8\%$). Comparison of the conventional SA and the proposed SA(τ_u) model.

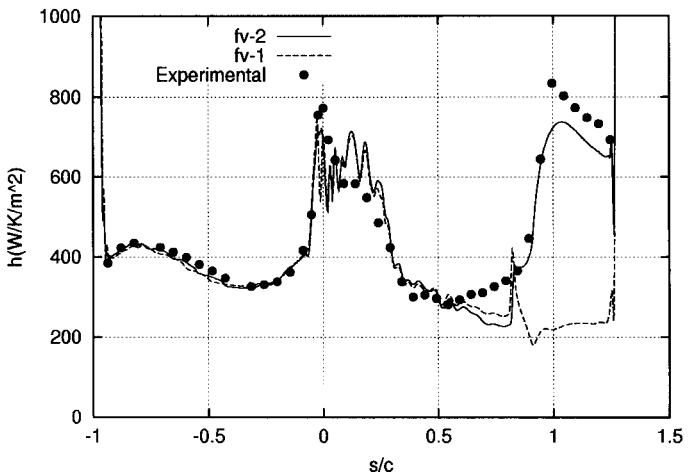

Figure 15. MUR235 ($Re = 2.65 \times 10^5$, $M_{2,is} = 0.927$, $Tu = 6.0\%$). Heat flux coefficient distributions using fv-1 and fv-2.

Figures 17, 18 and 19 illustrate the behavior of the proposed model at low, medium and high Reynolds numbers, respectively. In each of these figures, three cases are shown at low, medium and high free-stream turbulence intensities ($\tau_u = 1, 4$ or 6%). The AGS model was used for the $\tau_u = 1\%$ cases whereas any other case was treated through the Mayle model. In all cases, the predictions are in satisfactory agreement with the measurements. For the same inlet Reynolds number, the heat flux close to the leading edge stagnation point grows with the turbulence intensity and so does the heat flux. In the low Reynolds number cases, the heat

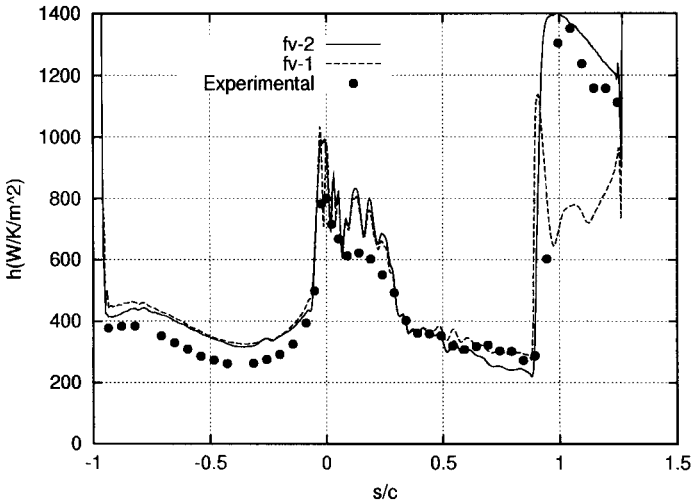

Figure 16. MUR247 ($Re = 4.87 \times 10^5, M_{2,is} = 0.922, Tu = 1.0\%$). Heat flux coefficient distributions using fv-1 and fv-2.

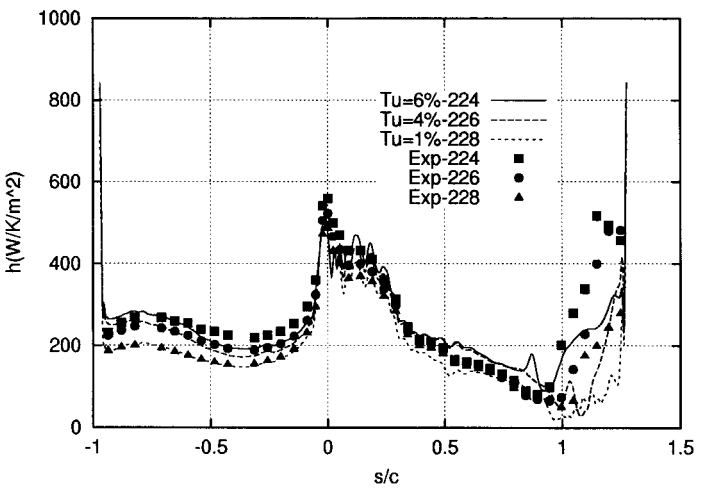

Figure 17. MUR228 ($Re = 1.36 \times 10^5$, $M_{2,is} = 0.933$, $Tu = 1\%$). MUR226 ($Re = 1.34 \times 10^5$, $M_{2,is} = 0.920$, $Tu = 4\%$), MUR224 ($Re = 1.36 \times 10^5$, $M_{2,is} = 0.927$, $Tu = 6\%$) Heat flux coefficient distributions for different Tu values at low Reynolds numbers.

flux distribution on the pressure side matches perfectly the experiments, even in the high-τ_u case. Transition occurs over the suction side close to the trailing edge but its onset moves slightly upstream for higher τ_u values. Both transition criteria predict well the location of the transition point, within their application range. Similar conclusions can also be drawn by examining the results shown in Figure 18. The flow behaves qualitatively in a similar manner but results in higher heat flux values, as expected.

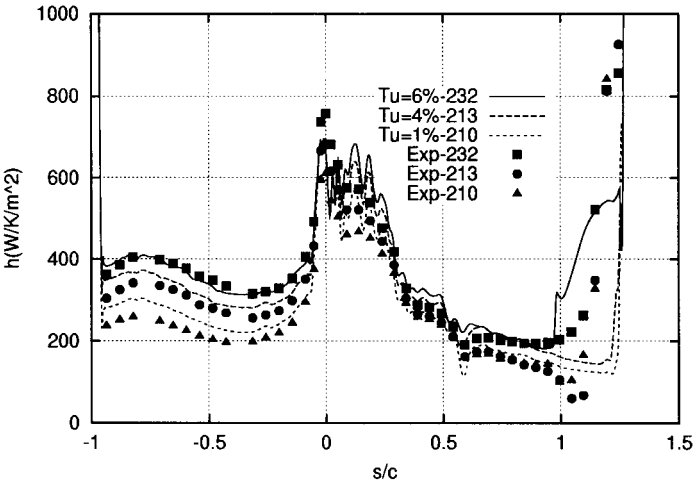

Figure 18. MUR210 ($Re = 2.43 \times 10^5$, $M_{2,is} = 1.076$, $Tu = 1\%$), MUR213 ($Re = 2.41 \times 10^5$, $M_{2,is} = 1.068$, $Tu = 4\%$), MUR232 ($Re = 2.42 \times 10^5$, $M_{2,is} = 1.061$, $Tu = 6\%$). Heat flux coefficient distributions for different Tu values at medium Reynolds numbers.

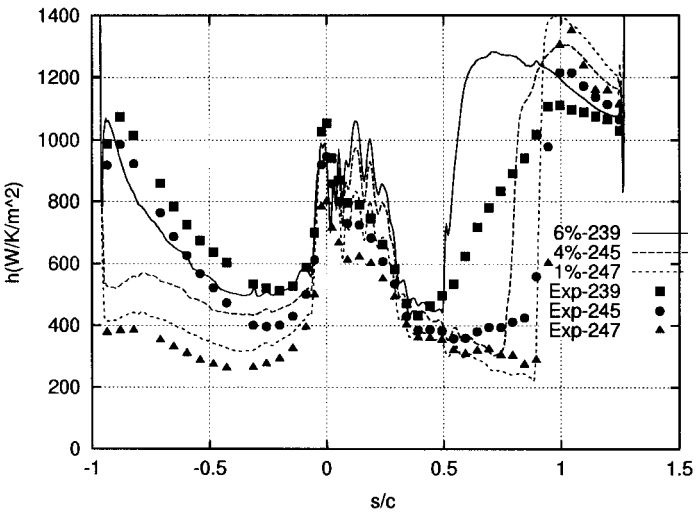

Figure 19. MUR247 ($Re = 4.87 \times 10^5$, $M_{2,is} = 0.922$, $Tu = 1\%$), MUR245 ($Re = 4.91 \times 10^5$, $M_{2,is} = 0.924$, $Tu = 4\%$), MUR239 ($Re = 4.92 \times 10^5$, $M_{2,is} = 0.922$, $Tu = 6\%$). Heat flux coefficient distributions for different Tu values at high Reynolds numbers.

The high Reynolds cases, Figure 19, are much more interesting since the onset of transition is located upstream on the suction side and the boundary layer developing along the pressure side is transitional over its major part. The SA(τ_u) model predicts transition at the correct location on the suction side. However, the increase in h is abrupt and deviates from the gradual increase that has been measured. On the pressure side, the transitional boundary layer

is captured well for the high-τ_u case but discrepancies exist in the $\tau_u = 4\%$ case. This could be attributed to the mild turbulence intensity and the appropriateness of the transition model (Mayle or AGS) for it. A transitional boundary layer was measured (similar to the $\tau_u = 6$ per cent), while our predictions gave a boundary layer which mostly resembles the $\tau_u = 1$ per cent distribution of the heat transfer coefficient. As expected, the pressure side curve is captured very satisfactorily in the low-τ_u case.

6. CONCLUSIONS

The flow in a 2D, high-pressure turbine nozzle guide vane cascade, at various operating conditions, has been analyzed using an enhanced variant of the Spalart–Allmaras model. The major modification consists of the introduction of an extra viscosity coefficient which is proportional to the free-stream turbulence and undergoes damping within the boundary layer. This modification proved to be adequate to overcoming a noticeable shortcoming of the Spalart–Allmaras model, i.e. the lack of sensitivity to the level of the free-stream turbulence intensity.

The enhanced Spalart–Allmaras model simulates transition with its own transition terms, in the expense of a separate algebraic criterion for the prediction of the onset of transition. As such, the Abu-Ghannam and Shaw and the Mayle criteria have been employed. Both yield satisfactory predictions within their calibration rates, namely for relatively low and high turbulence intensities, respectively.

Apart from the accurate prediction of the transition and the relevant increase in heat transfer over the suction side of the blade, the enhanced Spalart–Allmaras model gives excellent predictions on the pressure side as well. It is along the latter where algebraic, one- and two-equation turbulence models usually fail, especially whenever the free-stream turbulence is high.

Unstructured grids with triangular elements have been used; so, this paper proposes solutions that may overcome problems related to the 'lack of structure' in the grid. Since integral boundary layer quantities need to be computed, accurate interpolations are required along with a smoothing for the external velocity that is to be differentiated.

Finally, though not originally proposed herein, this work reconfirmed the advantages of using the containment-circle tessellation in any finite-volume scheme that involves highly stretched grid cells.

REFERENCES

1. Mayle RE. The role of laminar-turbulent transition in gas turbine engines. *Journal of Turbomachinery* 1991; **113**:509–537.
2. Arts T, de Rouvroit ML, Rutherford AW. Aero-thermal investigation of a highly-loaded transonic linear turbine guide vane cascade. A Test Case for Inviscid and Viscous flow Computations. VKI-Technical Note 174, September 1990.
3. Larsson J. Eriksson, Hall U. External Heat Transfer Predictions in Supersonic Turbines using the Reynolds Averaged Navier–Stokes Equations. ISABE 95-7101, 1995.
4. Hu J, Fransson TH. Numerical Performance of Transition Models in Different Turbomachinery Flow Conditions: A Comparative Study. ASME Paper 2000-GT-520, 2000.
5. Gehrer A, Jericha H. External heat transfer predictions in a highly loaded transonic linear turbine guide vane cascade using an upwind biased Navier–Stokes solver. *Journal of Turbomachinery* 1999; **121**:525–531.
6. Migliorini F, Michellassi V. Transition and heat transfer modelling in transonic linear cascades. *Proc. 2nd European Conference on Turbomachinery – Fluid Mechanics and Thermodynamics*, Antwerpen, Belgium, March 5–7, 1997.

7. Lefebvre M, Arts T. Numerical simulation of laminar/turbulent flows in a HP turbine linear cascade using unstructured grids. VKI-Reprint 1996-05 from *Seminar and Workshop on 3D Turbomachinery Flow Prediction* IV, Courchevel, France, January 8–11, 1996.
8. Larsson J. Two-Equation Turbulence Models for Turbine Blade Heat Transfer Simulations. ISABE 95-7163, 1997.
9. Abu-Ghannam BJ, Shaw R. Natural transition of boundary layer – the effect of turbulence, pressure gradient and flow history. *Journal of Mechanical Engineering Science* 1980; **22**(5):213–228.
10. Spalart PR, Allmaras SR. A One-Equation Turbulence Model for Aerodynamic Flows. AIAA Paper 92-0439, 1992.
11. Spalart P, Allmaras S. A one-equation turbulence model for aerodynamic flows. *La Recherche Aérospatiale* 1994; **1**:5–21.
12. Rumsey CL, Gatski TB, Ying SX, Bertelud A. Prediction of High-Lift Flows Using Turbulent Closure Models. AIAA Paper 97-2260, 1997.
13. Volino RJ. A new model for free-stream turbulence effects on boundary layers. *Journal of Turbomachinery* 1998; **120**:613–620.
14. Forrest AE. Engineering Predictions of Transitional Boundary Layers. AGARD-CP-224, 1977.
15. Boyle RJ. Navier–Stokes analysis of turbine blade heat transfer. *Journal of Turbomachinery* 1991; **113**:392–403.
16. Barth TJ. Numerical Aspects of Computing Viscous High Reynolds Number Flows on Unstructured Meshes. AIAA Paper 91-0721, Jan. 1991.
17. Roe P. Approximate Riemann solvers, parameter vectors, and difference schemes. *Journal of Computational Physics* 1981; **43**:357–371.
18. Anderson WK, Bonhaus DL. An implicit upwind algorithm for computing turbulent flows on unstructured grids. *Computers and Fluids* 1994; **23**(1):1–21.
19. Rodi W, Michellassi V, Gieb PA. Experimental and Numerical Investigation of Boundary-Layer and Wake Development in a Transonic Turbine Cascade. ASME Paper 97-GT-483, 1997.
20. White FM. *Viscous Fluid Flow*. McGraw-Hill: New York, 1991; 430.
21. Hu J, Fransson TH. On the Application of Transition Correlations in Turbomachinery Flow Calculations. ASME Paper 98-GT-460, 1998.
22. Dunham J. Predictions of Boundary Layer Transition on Turbomachinery Blades. AGARD-AG-164, 1972.

